

The inner radio jet region and the complex environment of SS433

Z. Paragi^{1,2}, R.C. Vermeulen³, I. Fejes¹, R.T. Schilizzi^{2,4}, R.E. Spencer⁵, and A.M. Stirling⁵

¹ FÖMI Satellite Geodetic Observatory, P.O. Box 546, H-1373 Budapest, Hungary

² Joint Institute for VLBI in Europe, P.O. Box 2, 7990 AA Dwingeloo, The Netherlands

³ Netherlands Foundation for Research in Astronomy, P.O. Box 2, 7990 AA Dwingeloo, The Netherlands

⁴ Leiden Observatory, P.O. Box 9513, 2300 RA Leiden, The Netherlands

⁵ Nuffield Radio Astronomy Laboratory, Jodrell Bank, Macclesfield, Cheshire, SK11 9DL, UK

Received 15 April 1999 / Accepted 28 June 1999

Abstract. We present multi-frequency VLBA+VLA observations of SS433 at 1.6, 5 and 15 GHz. These observations provide the highest angular resolution radio spectral index maps ever made for this object. Motion of the components of SS433 during the observation is detected. In addition to the usual VLBI jet structure, we detect two radio components in the system at an anomalous position angle. These newly discovered radio emitting regions might be related to a wind-like equatorial outflow or to an extension of the accretion disk. We show that the radio core component is bifurcated with a clear gap between the eastern and western wings of emission. Modelfitting of the precessing jets and the moving knots of SS433 shows that the kinematic centre – i.e. the binary – is in the gap between the western and eastern radio core components. Spectral properties and observed core position shifts suggest that we see a combined effect of synchrotron self-absorption and external free-free absorption in the innermost AU-scale region of the source. The spatial distribution of the ionized matter is probably not spherically symmetric around the binary, but could be disk-like.

Key words: stars: individual: SS433 – ISM: jets and outflows – radio continuum: stars

1. Introduction

SS433 is an eclipsing binary star which ejects antiparallel jets at a near relativistic velocity of 0.26c (e.g. Vermeulen 1995). The kinematics is revealed by optical Doppler-shifted lines (e.g. Margon & Anderson 1989), as well as radio maps e.g. the corkscrew-shaped trails due to precession (Hjellming & Johnston 1981). The jets show complicated precessing and nodding motions, they are collimated to better than 4°. The velocity of ejection is constant to within a few percent. Radio flux monitoring programmes showed that SS433 has active and quiescent periods (e.g. Fiedler et al. 1987). Knots in the jets moving at 0.26c can be seen on MERLIN scales (e.g. Spencer 1979, 1984). Radio structure on a scale of 10 to 50 mas was discovered in 1979 (Schilizzi et al. 1979). Since then, many VLBI observations have

been made with a variety of arrays and observing frequencies which revealed that moving components are present in both the active and quiescent periods of SS433 (e.g. Romney et al. 1987; Fejes et al. 1988; Vermeulen et al. 1993). These observations also showed that the central part of the radio source has a core-wing morphology which is not centre-brightened. The presence of a brightening zone – where the moving components become brighter – at 50 milliarcsecond from the centre was discovered by Vermeulen et al. (1993).

We present VLBI observations of SS433 at 1.6, 5 and 15 GHz. These observations provide us with the highest resolution spectral index maps ever made for this object. In addition to the usual VLBI structure, our maps show several new features in the system. In Sect. 2. we describe the observations and the data reduction process. In Sect. 3. the VLBI images and some related observational results are presented. We discuss our results in Sect. 4.

2. Observations, calibration and data reduction

The observations took place on 6 May 1995 with the VLBA and a single element of the VLA at 1.6, 5 and 15 GHz. At this time the binary orbital phase was 0.28 (where $\phi = 0$ corresponds to the eclipse of the accretion disk by the normal star) while the precession phase (following the definition of Vermeulen 1989) of the radio jets was 0.5, when the approaching jet lies closest to the line of sight. SS433 was observed during 10 hours using left circular polarization and 16 MHz bandwidth. The experiment included some phase-referencing scans with the background radio sources 1910+052 (at all frequencies) and 1916+062 (5 GHz only). Frequencies were cycled between 1.6, 5 and 15 GHz every 6.5 minutes except during the phase reference scans.

Initial data calibration was done using the NRAO AIPS package (Cotton 1995; Diamond 1995). We used measured antenna system temperatures for amplitude calibration. There was a need to fringe-fit for the delay and fringe rate for the outer antennas of the VLBA separately due to low signal-to-noise ratios on the longest baselines. Even with this method, solutions failed for the antennas MK and SC. We made a preliminary image using the rest of the array. After dividing the source model visibilities into the dataset we repeated the fringe-fitting as de-

Send offprint requests to: Z. Paragi, 1st address (paragi@sgo.fomi.hu)

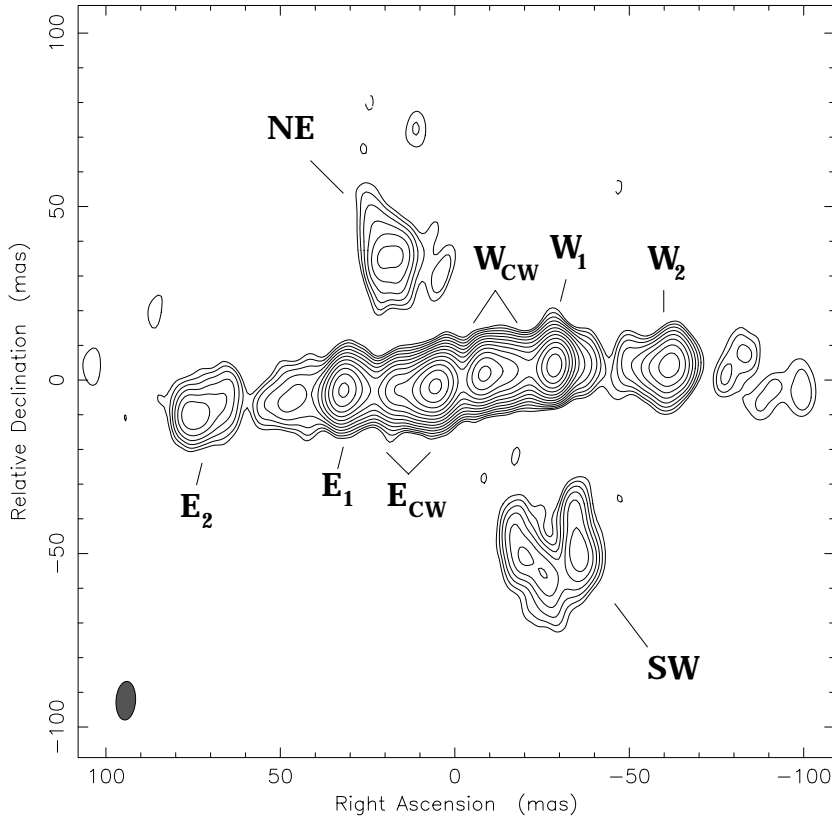


Fig. 1. Naturally weighted image of SS433 at 1.6 GHz. For clarity we indicate some components mentioned in the text. Contour levels are $-1.41, 1.41, 2.0, 2.83, 4.0, 5.66, 8.0, 11.31, 16.0, 22.63, 32.0, 45.25, 64.0, 90.51\%$ of the peak brightness of 53.3 mJy/beam, the restoring beam is 11.14×5.59 mas, $PA = -3.8^\circ$

scribed above, and were able to obtain solutions for all antennas except SC at 15 GHz. The complex bandpasses were calibrated using our fringe-finder sources 1803+784 and 3C454.3. After bandpass calibration, the data were averaged in frequency in each IF and then in time (one minute integration time). Editing, self-calibration and imaging was carried out using DIFMAP (Shepherd et al. 1994).

3. Results

3.1. Images

We present the naturally weighted images of SS433 at 1.6 GHz (Fig. 1.), 5 GHz, and 15 GHz (Fig. 2.). At 1.6 and 5 GHz there is the well-known jet structure, oriented largely East-West, which is roughly bi-symmetric in shape although not in detailed flux density. We have labelled some of the more prominent structures in accordance with our interpretation outlined below. By using a 50 mas restoring beam, we were able to trace the jets out to 500 mas from the centre at 1.6 GHz (Fig. 3.). The 1.6 GHz image in addition contains extended features in locations oriented at a large angle to the jets, where no emission has ever been seen before. We have performed extensive tests to verify that these are not artifacts of our data-reduction method. There is evidence for these same regions at 5 GHz, but they are too faint and too extended to be properly imaged from our data. The 15 GHz image is more asymmetric, but shows the same general inner jet structure: E_1 and W_1 are identifiable with the same separation as at the lower frequencies, and there is also emission at the

location of the E_{cw} and W_{cw} complexes. Clearly, all emission regions are extended, and the details of their morphology are difficult to image reliably at this high resolution.

Our resolution at 5 and 15 GHz was sufficient to detect the motion of some jet components during the 12 hours observing time. Source structure changes did not affect the final images significantly – this was checked by splitting the dataset into shorter timeranges. However, time-smearing may have affected the dynamic range of our images, especially at 15 GHz.

3.2. Alignment between frequencies

Components E_1 and W_1 , with their well-defined constant separation of 60 mas, are the most easily recognizable features between the three frequencies, and we have used these for the relative alignment of the images. We have been able to verify this relative alignment at 5 and 15 GHz by phase-referencing. SS433 and 1910+052 (an extragalactic background source located at an angular distance of $24'$) were observed alternately in short 1 min. (at 15 GHz) and 2 min. (at 5 and 1.6 GHz) cycles during four phase-referencing scans. We fringe-fitted 1910+052 using a point source model, and made an image. The resulting model visibilities were divided into the dataset and we repeated fringe-fitting. Delay, multiband-delay and fringe rate solutions – corrected for structural effects of the reference source – were applied to SS433. In this way images of SS433 at different frequencies are overlaid naturally - assuming that the 1910+052 image centres at different frequencies are exactly at the same place in the source. In agreement with our first estimates, the

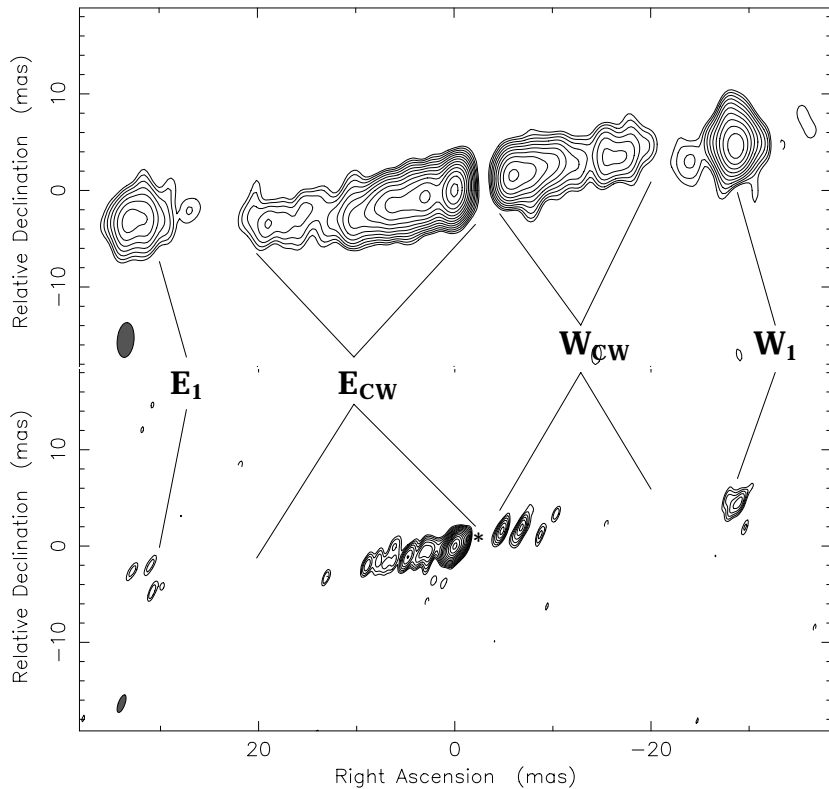


Fig. 2. Naturally weighted images of SS433 at 5 GHz (upper image) and 15 GHz (lower image). For clarity we indicate some components mentioned in the text. The kinematic centre is indicated by an asterisk in the 15 GHz image. Contour levels are $-1.41, 1.41, 2.0, 2.83, 4.0, 5.66, 8.0, 11.31, 16.0, 22.63, 32.0, 45.25, 64.0, 90.51\%$ of the peak brightness of 36.2 mJy/beam (5 GHz) and 50.1 mJy/beam (15 GHz). The restoring beam is 3.62×1.70 mas, $PA = -5.6^\circ$ and 1.94×0.67 mas, $PA = -20.0^\circ$, respectively

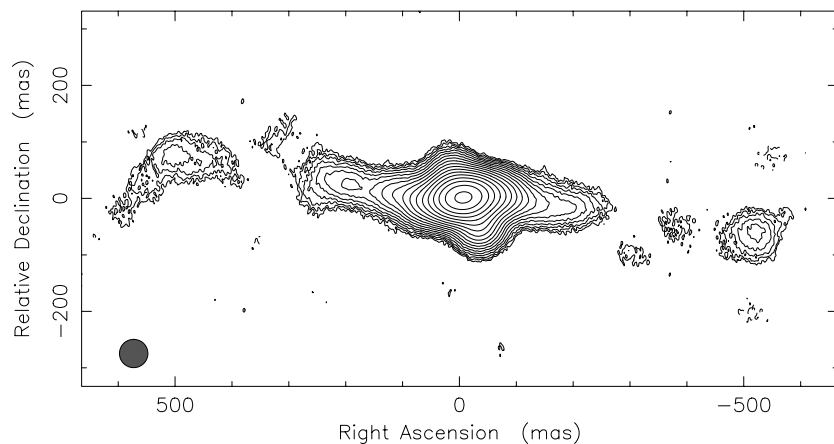


Fig. 3. The large scale structure of SS433 at 1.6 GHz. Contour levels are $-0.25, 0.25, 0.36, 0.50, 0.71, 1.0, 1.41, 2.0, 2.83, 4.0, 5.66, 8.0, 11.31, 16.0, 22.63, 32.0, 45.25, 64.0, 90.51\%$ of the peak brightness of 248.3 mJy/beam. The restoring beam is 50 mas

15 and 5 GHz images aligned well. Unfortunately, at 1.6 GHz the reference source turned out not to have compact structure, perhaps as a result of scattering, either in the supernova remnant W50, or elsewhere along the line of sight through our Galaxy.

The “absolute” centre of ejection, where the binary stellar system is located, is not obvious from the radio emission at any frequency, and there is no centrally brightened “core” feature. For example, we find that the brightest part of E_{cw} (on the side closest to the centre), is 4 mas closer to E_1 at 1.6 GHz than at 5 and 15 GHz. Also, the separation between the inner parts of E_{cw} and W_{cw} decreases from 14 mas, to 6 mas, and then to 5 mas, in going from 1.6 GHz, to 5 GHz, and then to 15 GHz.

However, we can use the well-established kinematic model of the precessing jets of SS433 (Margon & Anderson 1989;

Hjellming & Johnston 1981; Vermeulen 1989) to find the centre. We believe that the features E_1 - W_1 and E_2 - W_2 are matched pairs, corresponding to successive events of ejection or knot formation which occurred simultaneously in both jets. Adopting the kinematic model parameters of Margon & Anderson (1989) we find ages of 3.5 days and 7 days for E_1 - W_1 and E_2 - W_2 , respectively. The greater angular extent (i.e. apparent component spacing) on the Eastern (approaching) side is in accordance with the light travel time predictions of the kinematic model. Based on E_1 and W_1 in the 5 GHz image, we derive that the most plausible location of the centre is ~ 2.5 mas W and ~ 0.7 mas N of the peak of E_{cw} at 5 GHz.

While our main interest was not to improve the accuracy of the kinematic model parameters, we made a series of tests

Table 1. Flux densities of components. The coordinates of boxes in which the flux density was integrated are also given

Component	Flux density (mJy)			Box coordinates (mas)			
	1.6 GHz	5 GHz	15 GHz	x_1	y_1	x_2	y_2
E ₂	16.8	7.5	–	86.5	–23.5	58.5	18.0
E ₁	42.4	18.1	3.1	38.5	–18.0	23.0	12.5
E _{cw}	116.2	113.4	121.5	23.0	–16.0	–2.5	16.0
W _{cw}	76.1	44.3	17.4	–2.5	–13.0	–22.0	18.0
W ₁	56.6	33.0	9.5	–22.0	–9.5	–35.5	21.0
W ₂	25.6	9.9	–	–40.0	–11.0	–71.0	20.5
NE	19.7	6.0	–	31.0	18.5	–1.0	58.5
SW	32.6	10.5	–	–10.5	–72.5	–44.5	–24.5

at all frequencies in which we varied the projected position angle of the precession cone axis in the plane of the sky, and independently the model precession phase; acceptable values of these parameters are well correlated from our images. We find that the previously reported PA = 100±2° (e.g. Hjellming & Johnston 1981) fitted the structures well. Our main result is that the kinematic model centre is between E_{cw} and W_{cw}, in the middle of the core-complex in the 15 GHz image (see Fig. 2.).

3.3. Spectral index maps

We used the relative image alignments as described in Sect. 3.2. Shifting of the uv-data was performed by self-calibrating to model files brought into alignment using the Caltech VLBI Package (Pearson & Readhead 1984) MODFIX program. Spectral index maps between 1.6–5 GHz and 5–15 GHz were made in AIPS after convolving the higher frequency image with the lower frequency beam in both cases (Fig. 4.).

The central region has an inverted spectrum, $\alpha_{1.6}^5 = 1$ ($S \propto \nu^\alpha$ throughout this paper). Between 1.6 and 5 GHz, the jet spectral index steepens with distance from the core, decreasing below –1.0 at about 25 mas, while there are flatter regions, especially the knots at 30 mas. These knots, E₁ and W₁, differ in spectral properties, $\alpha_{1.6}^5 = -0.7$ for E₁, and $\alpha_{1.6}^5 = -0.3$ for W₁. In general, the two jets have similar spectral behaviour. This is not true between 5 and 15 GHz, where the western jet steepens much faster, reaching $\alpha_5^{15} = -1$ less than 10 mas from the core. In the 5–15 GHz image we clearly resolve the core gap. The eastern part consists of a large, inverted area ($\alpha_5^{15} = 0.5-0.65$), while to the West only a thin inverted edge can be seen ($\alpha_5^{15} \sim 0.5$).

3.4. Modelfitting and flux densities of the source components

We performed modelfitting in DIFMAP. We divided the 5 GHz dataset into three parts in order to fit the positions of the source components during the observation. The motion of E₁ and W₁ was detected, in agreement with the kinematic model. Our modelfitting results, however, are not accurate enough to investigate the proper motion of these components in detail, because the time interval is too short. We did not detect unambiguous motion in the inner jets. Note that there are no well separated components in the inner part of the jets, which makes the modelfitting process difficult.

As the source structure cannot be described with a single set of model components at all three frequencies, flux densities of the components were determined from the images in AIPS. We defined eight areas on the images (around E_{cw}, W_{cw}, ...) in which flux densities were summed up. These are listed in Table 1.

4. Discussion

4.1. The core region and the inner jets

Our observations confirm the result of Vermeulen et al. (1993) that the core area is not centre-brightened. For the first time, we have the resolution to see a gap between the core-wings (Figs. 1. and 2.). Kinematic modelling – based on the jet curvature and symmetry of outer components – showed that the kinematic centre of the source is in the middle of the gap in the 15 GHz image. The separation of the brightest parts of E_{cw} and W_{cw} increases with decreasing frequency as a result of synchrotron self-absorption, in rough accordance with various different jet models, described below. However, the spectral properties are quite dissimilar between E_{cw} and W_{cw}. It is obvious that their flux density ratio at any arbitrary frequency does not simply reflect the effect of differential Doppler-boosting as was thought to be the case by Fejes (1986) and Vermeulen (1989). We argue below that the different spectra are caused by free-free absorption in a medium which envelopes the various parts of the jets to different depths.

In the standard extragalactic jet model the distance of the self-absorbed radio core from the central engine is proportional to ν^{-1} (Blandford & Königl 1979); this leads to a predictable radio core position shift between frequencies. In the case of continuous jets (steady emission pattern) the arm-length ratio between the approaching and the receding jet is always unity, and the central engine is simply located mid-way between the radio “cores” in the two jets. Following the formalism of Lobanov (1998), the measure of core position shift can be calculated by:

$$\Omega_{r\nu} = 4.85 \cdot 10^{-9} \Delta r_{\text{mas}} D \frac{\nu_1^{1/k_r} \nu_2^{1/k_r}}{\nu_2^{1/k_r} - \nu_1^{1/k_r}}, \quad (1)$$

where Δr_{mas} is the observed core position shift between observing frequencies ν_1 and ν_2 (given in Hz), D is the distance to the source in parsecs. The parameter k_r is model dependent,

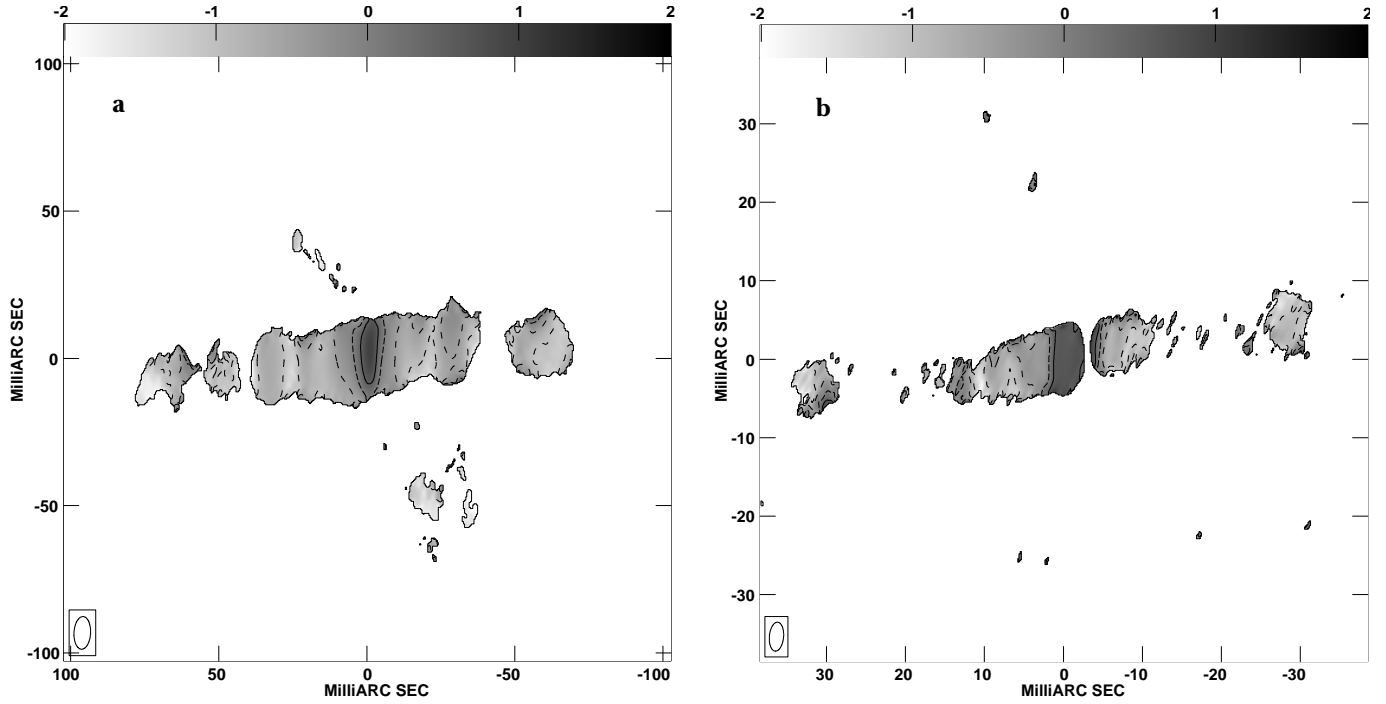


Fig. 4. Spectral index maps between **a** 1.6 and 5 GHz **b** 5 and 15 GHz. There are hints of emission near SW and NE on the restored 5 GHz image with spectral index ~ -1 . E_1 is also identified on the restored 15 GHz map. Contour levels in spectral index are $-1, -0.5, 0, 0.5$ ($S \propto \nu^\alpha$)

and was assumed to be unity. The equipartition magnetic field in the jet at 1 pc from the central engine can be written (Lobanov 1998):

$$B_1 = 2.92 \cdot 10^{-9} \left[\frac{\Omega_{r\nu}^3}{k_e \delta_j^2 \phi \sin^5 \theta} \right]^{1/4} \quad (2)$$

where δ_j is the jet doppler factor, ϕ is the jet opening angle and θ is the jet viewing angle. Using $B \propto r^{-1}$ with $k_e = 1$, substituting $\phi = 4^\circ$ for the jet opening angle, and calculating the parameters dependent on orientation (θ and δ_j) for precession phase 0.5, we find that the observed ~ 4 mas core position shift in the approaching jet side between 1.6 and 5 GHz results in an equipartition magnetic field strength $B = 0.4$ Gauss at 35 AU from the central engine, where the 1.6 GHz core component is observed.

As the separation of E_{cw} and W_{cw} between 1.6 and 5 GHz is proportional to ν^{-1} , and we obtained a reasonable field strength in our calculations, we conclude that the core-wings at 1.6 GHz are mainly self-absorbed. This seems to be in agreement with the fact that the integrated flux density of E_{cw} is nearly constant (Table 1.), i.e. the overall spectral index of the region is flat, as expected in case of synchrotron self-absorption. The peak brightness of the approaching jet at 15 GHz, however, does not seem to be high enough; the spectrum of a resolved, self-absorbed component would be more inverted. Moreover, the position shift between the 5 GHz and 15 GHz core components seems to be zero, or at least is smaller than our errors in aligning the images, which is estimated to be a few tenth of mas. We interpret the absence of core position shifts at high frequencies and the relative faintness of the high frequency near-in core

components in terms of additional free-free absorption. Increasing column depth of thermal electrons may result in a situation where the innermost part of E_{cw} at 15 GHz is absorbed so that the peak brightness is shifted outward from the central engine. Similarly, the brightest parts of the receding jet (located consecutively closer to the central engine with increasing frequency) are absorbed, and so the overall spectrum of W_{cw} remains steep from 1.6 GHz to 15 GHz.

We also compared the observed jet intensity profiles (i.e. the jet brightness distribution as a function of distance to the central engine) to the conical jet model of Hjellming & Johnston (1988). In this model the jet is assumed to expand adiabatically and the expansion is dominated by lateral motions of the flow. We also assumed that the expansion is free, and not slowed down by the interstellar medium. In agreement with our interpretation above, we obtained good first order agreement at 1.6 GHz between the shape of the observed and model jet intensity profiles. This further supports that E_{cw} and W_{cw} are regions in transition from optically thick to optically thin regimes. The effect of Doppler-boosting and de-boosting of the approaching and receding jet sides was also as expected. However, this is not the case at 5 GHz and 15 GHz. We scaled the model to the 1.6 GHz data, then estimated the additional free-free absorption required to explain the observed jet profiles at higher frequencies. As this is very sensitive to the alignment of the model with the data in position and the relative alignment of the jet intensity profiles between the frequencies – keeping in mind that we have a few tenth of mas uncertainty in aligning the images –, the values determined below must be considered as rough estimates. Note

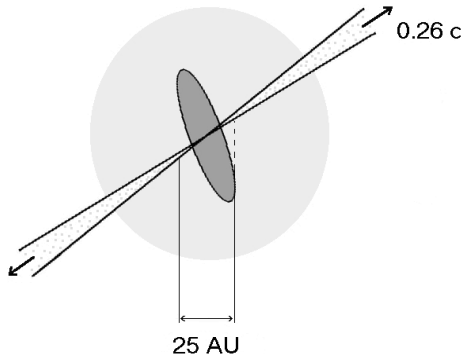


Fig. 5. A schematic view of the free-free absorbing medium around SS433. The density of free electrons increases sharply towards the central engine. At 15 GHz the absorbing cloud becomes optically thick at a projected distance of ~ 12.5 AU to the central engine (indicated by the inner shaded area), where τ_{ff} exceeds 3 for the receding jet. The large asymmetry between the two sides and the sudden increase in optical depths is most probably due to a disk-like geometry

also that these values are specific to the Hjellming & Johnston (1988) adiabatic jet model.

The optical depths required to explain the observed peak flux densities at 5 GHz are estimated to be $\tau_{\text{ff}} = 1$ and 2 at the approaching and the receding side, respectively. As there is a difference in the optical depths on the two sides, this additional absorption cannot be intrinsic to the jets. The required density of free electrons to produce $\tau_{\text{ff}} = 1$ at 5 GHz is $n_e = 2.2 \times 10^5 \text{ cm}^{-3}$ (assuming a thermal component with $T \sim 10^4$ K, and a characteristic pathlength $L=30$ AU through the absorbing medium). The relative faintness of E_{cw} at 15 GHz and the fact that W_{cw} is absorbed almost completely suggest that the column density increases toward the central engine. The almost completely absorbed peak of W_{cw} component at 15 GHz requires $n_e \sim 1.2 \times 10^6 \text{ cm}^{-3}$ or higher. We could not interpret our observations as the result of free-free absorption in a spherically symmetric stellar wind of the early-type star (Stirling et al. 1997). Assuming a spherically symmetric configuration and e.g. $n_e \propto r^{-3}$ dependence of the free electron density on the distance to the binary, the differences in the integrated emission measures cannot explain the observed high difference in the optical depths between the two sides. Instead we suggest the possibility of a disk-like geometry for the absorbing medium (Fig. 5). Note that this region is much larger than the accretion disk. The projected size of the gap between E_{cw} and W_{cw} is 25 AU, whereas the binary system is generally thought to be ~ 1 AU in size. The spherically symmetric versus equatorially enhanced stellar wind scenarios will be studied in multi-epoch multi-frequency monitoring observations spanning various phases of the precession cycle of SS433 which allow different lines of sight to be probed.

4.2. The anomalous emission regions NE and SW

Random projected velocity deviations of about 5000 km s^{-1} are frequently observed in the jets of SS433; these have in the

past been successfully explained by deviations of only a few degrees in the pointing angle of the jets (“jitter”). Detections of anomalous radio emission components have been reported in some cases. Modelfitting of 1981 single-baseline Effelsberg-Westerbork data (Romney et al. 1987) indicated an elongated structure straddling the core in PA 62° which is beyond the kinematic model cone. Spencer & Waggett (1984) showed anomalous radio emission $15\text{--}20^\circ$ from the predicted locus in a 1982 series of EVN 5 GHz images. Jowett & Spencer (1995) found a pair of knots apparently moving at only half the predicted jet velocity in a 1991 and 1992 series of 5 GHz MERLIN.

Our observation of SS433 shows two faint, extended emission regions to the NE and SW from the central engine – assumed to be located in between E_{cw} and W_{cw} components as explained above – extending in PA $\sim 30 \pm 20^\circ$ over a distance of 30 mas to 70 mas in the 1.6 GHz image (Fig. 1.). They are quite distinct from the “normal” jets, which are obviously also present. Features this far away in position angle from the jets have never been observed before.

The implied brightness temperature of 10^7 K suggests non-thermal radiation. Should the NE and SW components be moving approximately along the plane of the sky at $0.26c$ (like the jets), then these newly discovered features would have an age of a few days. But because this would imply an unprecedentedly large deviation from the kinematic model, because there were no noteworthy radio events in the source right before the observation (Fender et al. 1997), and, most importantly, because we have seen the features again in more recent data, with similar disposition (Paragi et al. in preparation), we believe that NE and SW are probably not anomalous knots which can be associated with the jets, ejected at near relativistic speeds. Instead, we believe these radio features are longer-lived, perhaps even permanent regions of emission extended along the equatorial plane of the binary system. We think they have not been previously detected because our VLBI array had an unprecedented sensitivity to extended, low surface brightness emission.

If we associate the anomalous components with a quasi-equatorial outflow from the system with typical early-type stellar wind speeds (in the order of 1000 km s^{-1}), we may observe the position angle of the flow to be correlated with the precessional phase. The possibility of such an outflow or extended disk around SS433 have been reported by several authors as summarized below.

The asymmetric and variable shape of the optical lightcurve of SS433 was explained by Zwitter et al. (1991) as being due to the effect of an optically thick disk-like outflow of matter extending more or less radially from the “slaved” accretion disk which is thought to surround the compact object in SS433. Slaved accretion disk models, in which different parts are in different planes because the matter is slaved to the rotation of the companion on which it originated, have already been invoked for SS433 by several authors (e.g. van den Heuvel 1981) soon after its discovery.

Zwitter et al. (1991) proposed a relatively large ($\sim 20^\circ$) opening angle to the *excretion flow*, centred close to the orbital plane of the binary system. The presence of a very extended

disk around SS433 (outer radius 1–3 arcmin, which translates to a few parsecs at the distance of the source) with an opening angle as large as $\sim 60^\circ$ based on geometrical considerations was invoked by Fabrika (1993).

The properties of Doppler shifted X-ray lines as a function of the precession phase observed by Brinkmann et al. (1991) and Kotani et al. (1996) also indicate the need for a slaved disk model. In their model, there is an extended rim of the accretion disk. However, the outer part of this disk must turn toward the orbital plane. So the opening angle of the extended envelope must be less than determined by Fabrika (1993).

According to numerical simulations by Sawada et al. (1986) a considerable fraction of the transferring gas is lost in a binary system through the L_2 Lagrangian point, behind the compact star. This results in an expanding envelope at $PA=10^\circ$. Numerical simulations applied directly to SS433 also suggested the existence of an equatorial outflow due to spiral shocks in the accretion disk (Chakrabarti & Matsuda 1992). This quasi-stationary spiral shock structure can also explain the subday variabilities observed in the optical part of the spectrum (Chakrabarti & Matsuda 1992).

We interpret NE and SW as the manifestation of the excretion disk in the radio regime. During episodes of enhanced mass transfer from the companion to the compact object, bright components emerge from the core-complex (Vermeulen et al. 1993). This may also lead to enhanced ejection into the excretion flow through the L_2 Lagrangian point, and develop shock waves into the ISM. Relativistic electrons can be produced in the shock fronts that are responsible for the observed non-thermal radiation. The observed position angle and the large extent of NE and SW are in agreement with the slaved disk model discussed above.

5. Conclusion

We have shown that SS433 is active even in its “low” state. There is a continuous inner jet region, and moving pairs of blobs are present. The eastern and western part of the core-complex is separated by a gap, which is in fact the kinematic model centre. There are fainter extended regions not connected directly to the moving jets of the source. We overview the models that explain the various activities observed in the system. We find that the slaved accretion disk scenario - in general - is in agreement with our observations. However, many questions remain to be answered. The asymmetry within the core implies that the radio emission and absorption scenario is not well established in SS433. On one hand, it is clear that there must be an intrinsic asymmetry in the free-free absorbing medium. On the other hand, we can not explain the spectral properties of the core-wings with a simple model. Multifrequency monitoring of SS433 at different precessional phases will hopefully help us to separate the effect of Doppler-boosting and viewing angle from intrinsic properties, and to constrain the spatial extent of

the absorbing medium in the innermost part of the source. The appearance of the extended disk also has to be monitored in further VLBI observations at low frequencies.

Acknowledgements. ZP wishes to acknowledge support for this research by the European Union under contract CHGECT 920011, the Netherlands Organization for Scientific Research (NWO), the Hungarian Space Office, and hospitality of JIVE and NFRA where part of this work has been carried out. We are grateful to the staff of the VLBA, the NRAO correlator for their support of our project. The National Radio Astronomy Observatory is operated by Associated Universities, Inc. under a Cooperative Agreement with the National Science Foundation.

References

- Blandford R.D., Königl A., 1979, *ApJ* 232, 34
 Brinkmann W., Kawai N., Matsuoka M., Fink H.H., 1991, *A&A* 241, 112
 Chakrabarti S.K., Matsuda T., 1992, *ApJ* 390, 639
 Cotton W.D., 1995, In: Zensus J.A., Diamond P.J., Napier P.J. (eds.) *Very Long Baseline Interferometry and the VLBA*. ASP Conference Series 82, 189
 Diamond P.J., 1995, In: Zensus J.A., Diamond P.J., Napier P.J. (eds.) *Very Long Baseline Interferometry and the VLBA*. ASP Conference Series 82, 227
 Fabrika S.N., 1993, *MNRAS* 261, 241
 Fejes I., 1986, *A&A* 166, L23
 Fejes I., Schilizzi R.T., Vermeulen R.C., 1988, *A&A* 189, 124
 Fender R.P., Bell Burnell S.J., Waltman E.B., 1997, *Vist. Ast.* 41, 3
 Fiedler R.L., Johnston K.J., Spencer J.H., et al., 1987, *AJ* 94, 1244
 Hjellming R.M., Johnston K.J., 1981, *ApJ* 246, L41
 Hjellming R.M., Johnston K.J., 1988, *ApJ* 328, 600
 Jowett F.M., Spencer R.E., 1995, In: Green D.A., Steffen W. (eds.) *Proc. 27th YERAC*, Cambridge University Press
 Kotani T., Kawai N., Matsuoka M., Brinkmann W., 1996, *PASJ* 48, 619
 Lobanov A.P., 1998, *A&A* 330, 79
 Margon B., Anderson S.F., 1989, *ApJ* 347, 448
 Pearson T.J., Readhead A.C.S., 1984, *ARA&A* 22, 97
 Romney J.D., Schilizzi R.T., Fejes I., Spencer R.E., 1987, *ApJ* 321, 822
 Sawada K., Matsuda T., Hachisu I., 1986, *MNRAS* 219, 75
 Schilizzi R.T., Norman C.A., van Breugel W., Hummel E., 1979, *A&A* 79, L26
 Shepherd M.C., Pearson T.J., Taylor G.B., 1994, *BAAS* 26, 987
 Spencer R.E., 1979, *Nat* 282, 483
 Spencer R.E., 1984, *MNRAS* 209, 869
 Spencer R.E., Waggett P., 1984, In: Fanti R. (ed.) *Proc. IAU Symposium* 110, p. 297
 Stirling A.M., Spencer R.E., Watson S.K., 1997, *Vist. Ast.* 41, 197
 van den Heuvel E.P.J., 1981, *Vist. Ast.* 25, 95
 Vermeulen R.C., 1989, Ph.D. Thesis, Leiden University
 Vermeulen R.C., 1995, In: W. Kundt (ed.) *Jets from Stars and Galactic Nuclei*. Springer Verlag, p. 122
 Vermeulen R.C., Schilizzi R.T., Spencer R.E., Romney J.D., Fejes I., 1993, *A&A* 270, 177
 Zwitter T., Calvani M., D’Odorico S., 1991, *A&A* 251, 92